Electrical Conductors

Deutsche Ausgabe: DOI: 10.1002/ange.201600029
Internationale Ausgabe: DOI: 10.1002/anie.201600029

Superior Electrical Conductivity in Hydrogenated Layered Ternary Chalcogenide Nanosheets for Flexible All-Solid-State Supercapacitors

Xin Hu[+], Wei Shao[+], Xudong Hang, Xiaodong Zhang, Wenguang Zhu, and Yi Xie**

Abstract: *As the properties of ultrathin two-dimensional (2D) crystals are strongly related to their electronic structures, more and more attempts were carried out to tune their electronic structures to meet the high standards for the construction of next-generation smart electronics. Herein, for the first time, we show that the conductive nature of layered ternary chalcogenide with formula of Cu_2WS_4 can be switched from semiconducting to metallic by hydrogen incorporation, accompanied by a high increase in electrical conductivity. In detail, the room-temperature electrical conductivity of hydrogenated-Cu_2WS_4 nanosheet film was almost 10^{10} times higher than that of pristine bulk sample with a value of about $2.9\times 10^4\ S\,m^{-1}$, which is among the best values for conductive 2D nanosheets. In addition, the metallicity in the hydrogenated-Cu_2WS_4 is robust and can be retained under high-temperature treatment. The fabricated all-solid-state flexible supercapacitor based on the hydrogenated-Cu_2WS_4 nanosheet film shows promising electrochemical performances with capacitance of 583.3 $F\,cm^{-3}$ at a current density of 0.31 $A\,cm^{-3}$. This work not only offers a prototype material for the study of electronic structure regulation in 2D crystals, but also paves the way in searching for highly conductive electrodes.*

Ultrathin two-dimensional (2D) crystals are valuable materials with various potential applications and fundamental theoretical interest.[1–10] They are ideal building blocks for the design of next-generation electronics with the combination of transparency, ultrathin thickness and flexibility[3,4] and show unique density of states near the Fermi level with respect to their corresponding bulk samples, thus exhibiting unprecedented properties.[5,6] In the past decade, accompanied by the booming development of graphene and its derivatives, much attention was paid to ultrathin nanosheets of inorganic graphene analogues (IGA) with rich electronic structures.[7] Among the various inorganic graphene analogues, the layered transition-metal chalcogenides (TMCs) garnered great research interest. TMCs can be insulators, semiconductors, half-metals, or metals, depending on their elemental composition.[8–10] With a weak van der Waals force between the layers, the layered TMCs can be easily exfoliated into single- or few-layer nanosheets, which find potential application in various areas, such as nanoelectronics, energy storage and electrocatalysis.[8–10] However, most of the two-dimensional materials show low electrical conductivity, which hampers their practical applications.[11–13]

Many efforts were made to tune the electrical transport behavior of 2D crystals to optimize their intrinsic conductivity. For example, external electric field or biaxial strain can induce the semiconductor-to-metal transition in bilayer MoS_2.[8] Chen et al. have shown that partially hydrogenated zigzag BN nanoribbons exhibit a series of transitions in electronic structures from semiconductor to half-metal, and then to metal depending on the hydrogen concentration.[14] In addition, the conductive nature of layered MoS_2/WS_2 could transform from semiconducting 2H phase to metallic 1T phase during the chemical exfoliation process, and the as-obtained 1T nanosheets show superior electrocatalytic hydrogen evolution ability.[9,15] Although many theoretical studies have been carried out on how to control the electronic structure in 2D crystals, experimental realization is difficult as harsh conditions are required, and the underlying principles are still unclear.[16,17]

Due to their rich electronic structures and diverse chemical compositions, the layered transition-metal chalcogenides offer ideal platforms to search for highly conductive 2D crystals by electronic structural control, and to understand their mechanisms. Currently, research interests on layered TMCs were expanded from the binary compounds to ternary or multiple-valued counterparts, who show richer electronic structures.[18–20] Herein, we investigate the ternary chalcogenides with formula of Cu_2MX_4 (M = Mo, W; X = S, Se), which possess a layered structure with weak van der Waals forces between the layers.[21] As a typical semiconductor, layered Cu_2MX_4 has been applied in photocatalysis[22] and electrochemical hydrogen evolution,[20] while rare attention was paid on its intriguing electronic structures. By taking Cu_2WS_4 as example, we show here, for the first time, that its conductive nature can be strongly modified by hydrogenation, that is, a transition from semiconductor to metal. Benefiting from its high electrical conductivity and ultrathin thickness, the hydrogenated-Cu_2WS_4 nanosheets were applied as electrode for the construction of a all-solid-state flexible supercapacitor. The as-fabricated supercapacitor achieves high electrochemical performances, demonstrating the metallic hydrogenated-Cu_2WS_4 nanosheets to be promising candidate for the design of portable electronics.

The hydrogenated-Cu_2WS_4 nanosheets were obtained by a lithium intercalation assisted exfoliation strategy, illustrated

[*] Dr. X. Hu,[+] W. Shao,[+] X. D. Hang, Dr. X. D. Zhang, Prof. W. G. Zhu, Prof. Y. Xie
Hefei National Laboratory for Physical Science at Microscale, Collaborative Innovation Center of Chemistry for Energy Materials, University of Science and Technology of China
Hefei, Anhui, 230026 (P.R. China)
E-mail: zhxid@ustc.edu.cn
yxie@ustc.edu.cn
[+] These authors contributed equally to this work.

Supporting information for this article can be found under: http://dx.doi.org/10.1002/anie.201600029.

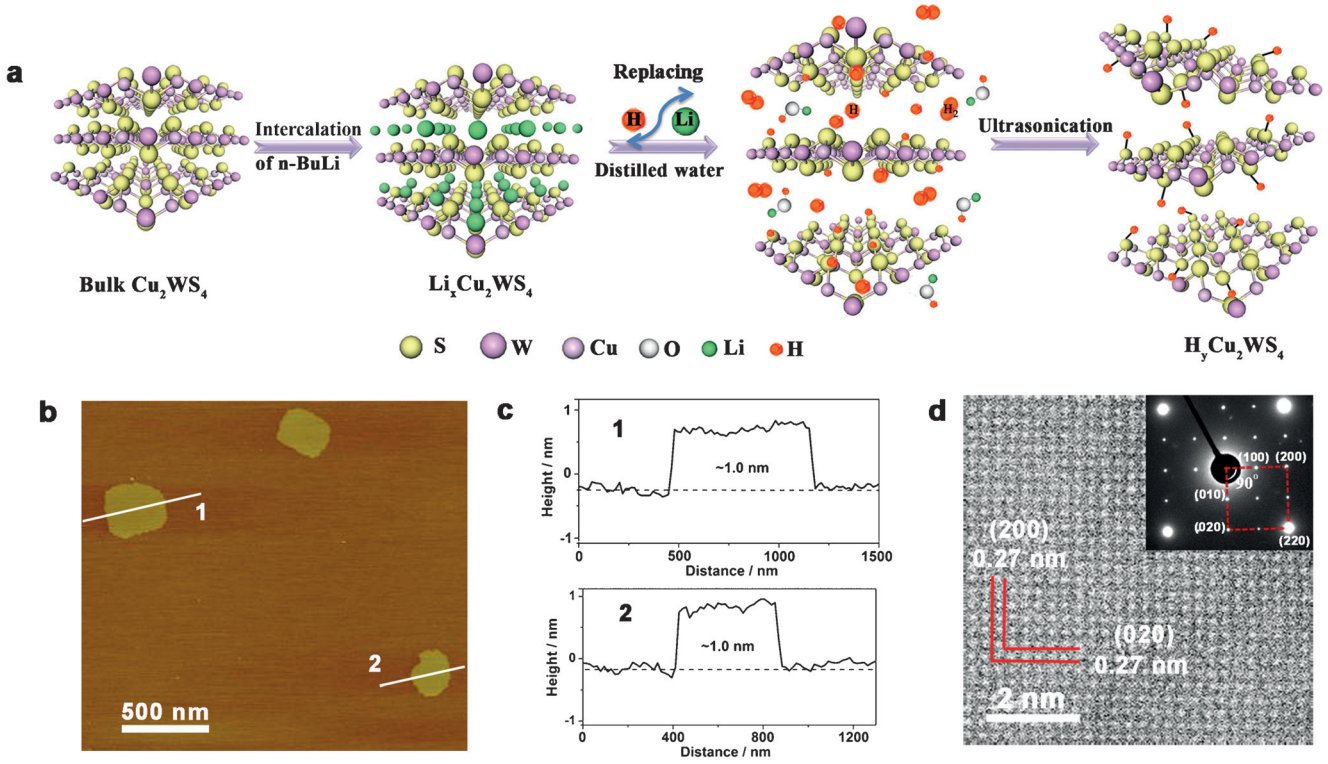

Figure 1. a) Formation of hydrogenated-Cu_2WS_4 nanosheets. b) AFM image of the as-obtained nanosheets. c) Corresponding height diagram. d) HRTEM image and SAED pattern of the as-obtained nanosheets.

in Figure 1a. An intermediate precursor of $Li_xCu_2WS_4$ was obtained by treating the bulk Cu_2WS_4 with n-butyllithium undergoing a lithium intercalation process, accompanying with weakened layer interaction. The formation of $Li_xCu_2WS_4$ plays a crucial role in the exfoliation and further hydrogen doping processes. In further treatment, the $Li_xCu_2WS_4$ would undergo a hydrolysis reaction ($Li_xCu_2WS_4 + H_2O \rightarrow H_2\uparrow + LiOH + H_yCu_2WS_4$) by replacing lithium with hydrogen atom in water, during which parts of the hydrogen incorporate into the exfoliated Cu_2WS_4 structure to form the ultrathin hydrogenated nanosheets. The morphology of the as-prepared nanosheets was revealed by transmission electron microscopy (TEM) and tapping mode atomic force microscopy (AFM) images as shown in Figure S2 (Supporting Information) and Figure 1b, respectively, where the free-standing nanosheets with sizes of a few hundred nanometers can be clearly observed. As shown in Figure 1c, the thickness of the nanosheets measured by AFM is about 1.0 nm, in good agreement with the unit cell of body-centered Cu_2WS_4 (*I*-Cu_2WS_4) along the *c*-axis. High-resolution TEM (HRTEM) and selective area electron diffraction (SAED) were performed on a typical nanosheet (Figure 1d) and reveal its single-crystalline nature. The lattice fringes of about 0.27 nm correspond to the plane distance of d_{200} and d_{020} of Cu_2WS_4 structure, confirming the exposure of *ab*-plane of the ultrathin nanosheet. The angle of adjacent spots in SAED pattern of 90° is matched well with theoretical value of the angle between (200) and (020) planes of *I*-Cu_2WS_4. The HRTEM analysis indicates that the as-exfoliated nanosheets retain the structure of Cu_2WS_4.

The structure of the as-exfoliated nanosheets was further studied by X-ray diffraction (XRD) and Raman spectroscopy, both of which can provide direct phase information of samples. As shown in Figure 2a, the XRD pattern of bulk materials can be readily indexed to tetragonal *I*-Cu_2WS_4 with cell parameters of $a = 5.444$ Å, $c = 10.068$ Å.[23] In comparison, only single diffraction peak of (002) facet for *I*-Cu_2WS_4 can be clearly observed for the as-assembled nanosheet film, indicating its highly *c*-orientation. Raman spectra give further evidence that there are no structural transformations during the lithium intercalation assisted exfoliation. As can be seen from Figure 2b, Raman spectra of both bulk Cu_2WS_4 and as-exfoliated nanosheets show three prominent peaks (A_1 mode, B_1 mode, and E mode)[24] with similar Raman shifts, thus indicating that the exfoliated nanosheets retain the structure of the bulk sample. Compared to the bulk sample, the E mode of exfoliated nanosheets located at 433.5 cm^{-1} is shifted to lower wavenumber by 17 cm^{-1}. The shift of Raman modes between bulk and thin nanosheets is a common phenomenon, which can be ascribed to the phonon confinement effect.[7]

The presence of hydrogen doping in the exfoliated nanosheets could be clearly identified by ^1H solid-state NMR spectroscopy and X-ray photoelectron spectroscopy (XPS). As displayed in the ^1H NMR spectra (Figure 2c), there are four peaks at 1.06, 3.52, 4.97 and 6.5 ppm for the exfoliated nanosheets, named as δ_1, δ_2, δ_3 and δ_4, respectively. Compared with as-exfoliated nanosheets, the bulk sample only shows a small single peak at 6.5 ppm, which can be ascribed to adsorbed water molecules. Because of the large surface area of as-exfoliated nanosheets, they can absorb

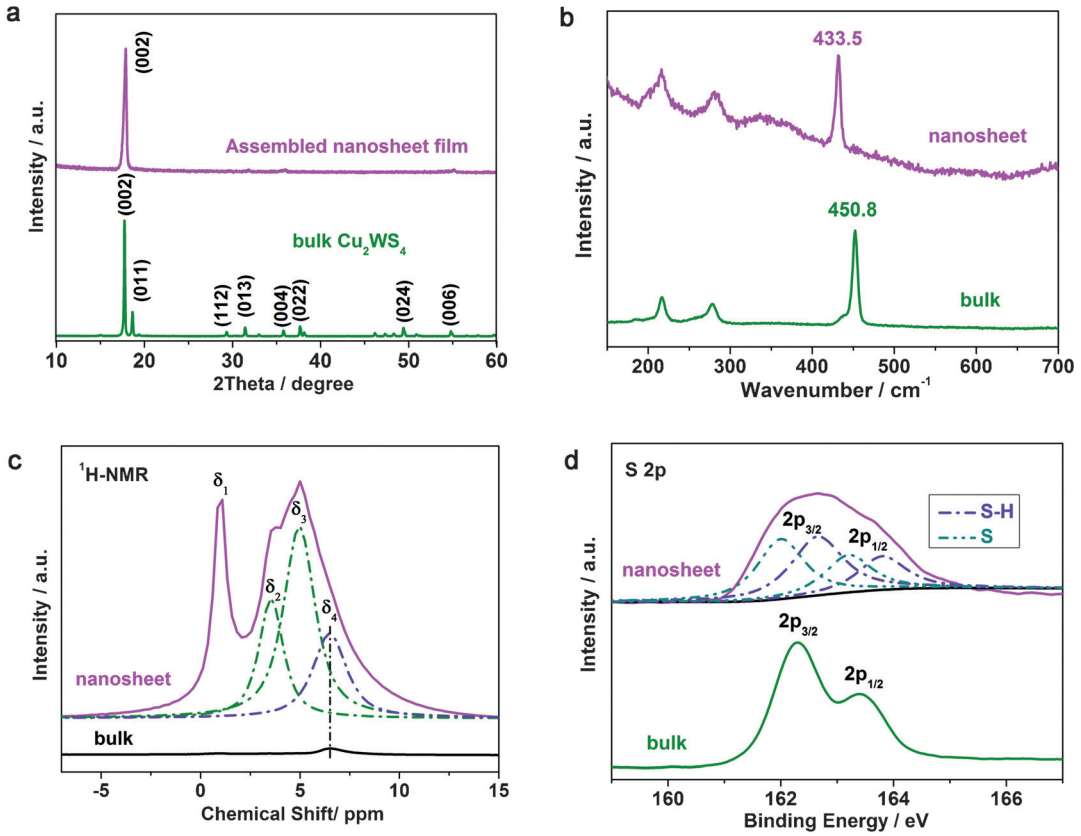

Figure 2. a) XRD pattern of the as-assembled hydrogenated-Cu_2WS_4 nanosheet film and bulk sample, revealing the high *c*-orientation of the exfoliated nanosheets. b) Raman spectra of hydrogenated-Cu_2WS_4 nanosheets and bulk sample under a 785 nm laser. c) H^1 solid-state NMR spectrum of the hydrogenated-Cu_2WS_4 nanosheets and bulk sample. δ_2 and δ_3 are the signals for S–H bonds; δ_1 and δ_4 are the signals for adsorbed butyl groups and water molecules, respectively. d) XPS of S 2p core level peak regions for hydrogenated-Cu_2WS_4 nanosheets and bulk sample.

more water molecules than the bulk sample, resulting in a stronger NMR signal at 6.5 ppm. In addition to water, the as-exfoliated nanosheets also adsorb butyl groups during the exfoliation process, as evidenced by the NMR signal at 1.06 ppm. The other two peaks at 3.52 and 4.97 ppm correspond to S–H bonds, giving direct evidence for the presence of hydrogen doping in the as-exfoliated nanosheets.[25] Herein, the two S–H bond signals indicate the existence of two hydrogen sites in the $H_yCu_2WS_4$ structure. In addition, as shown by XPS of S 2p (Figure 2d), there are two types of sulfur in the exfoliated nanosheets (pristine and hydrogenated), while the bulk sample only shows one type, further confirming that parts of sulfur in Cu_2WS_4 structure were hydrogenated during exfoliation. The results provide solid evidence of the hydrogen incorporation in ultrathin *I*-Cu_2WS_4 nanosheets, which maintains the structure of their bulk counterpart.

It is well known that hydrogen incorporation strongly affects the electronic structure of materials by providing external electrons, and it would be interesting for us to investigate the influence of hydrogen incorporation on the electrical transport properties of Cu_2WS_4. According to a previous report, *I*-Cu_2WS_4 is a typical semiconductor with an energy gap of about 2.0 eV (Figure S4).[22] The room-temperature resistivity of bulk Cu_2WS_4 was determined be $10^5\,\Omega\,m$ (calculated from the measured resistance of about $10^8\,\Omega$), which is so high that the value exceeds the limitation of our temperature-dependent resistivity test apparatus. In comparison, to our surprise, the electrical resistivity of the hydrogenated-Cu_2WS_4 nanosheet film was almost 10^{10} times lower than that of the bulk sample with a value of $3.45\times10^{-5}\,\Omega\,m$ at room temperature. Furthermore, as can be seen from Figure 3a, the electrical resistivity of the hydrogenated-Cu_2WS_4 nanosheet film increased with increasing temperature with $d\rho/dT>0$, exhibiting a typical metallic behavior. The results clearly show that the conductive nature of pristine bulk Cu_2WS_4 was strongly switched from semiconducting to metallic by hydrogen incorporation. The electrical conductivity of the hydrogenated-Cu_2WS_4 nanosheet film of about $2.9\times10^4\,S\,m^{-1}$ at room temperature is among the best recorded values for solution-assembled 2D thin films,[11–13] suggesting promising applications, for example as conductive electrodes.

The Hall coefficient (R_H) was further measured to study the charge transport properties of the hydrogenated-Cu_2WS_4 nanosheet film. As illustrated in Figure 3b, the nanosheet film shows a negative R_H at all tested temperatures, indicating that the charge carriers of hydrogenated-Cu_2WS_4 nanosheet are electrons. In addition, the value of R_H is very stable, showing no obvious change over the temperature range investigated.

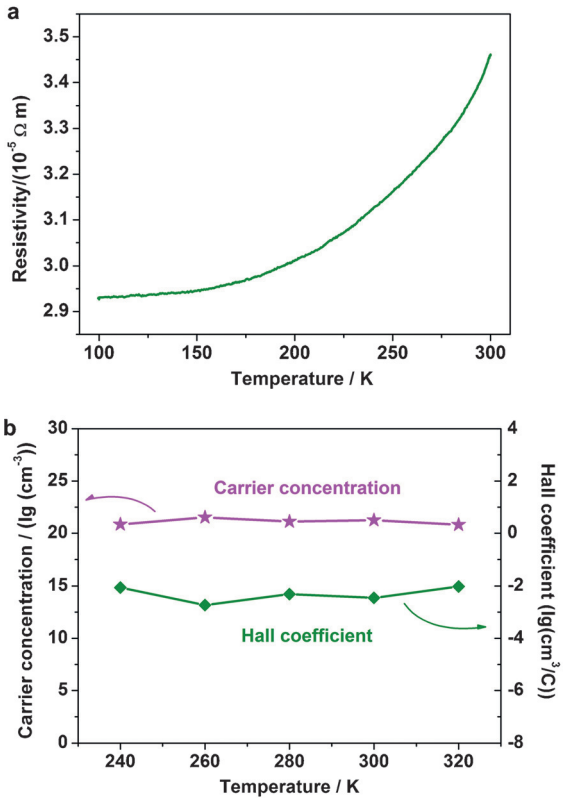

Figure 3. a) Temperature-dependent electrical resistivity. b) Temperature-dependent carrier concentration and Hall coefficient.

The carrier concentrations derived from the Hall coefficient show a constant value of about 6×10^{20}, which further confirms the metallic character of the hydrogenated-Cu_2WS_4 nanosheet. As can be seen from Figure S5, the photoluminescence of Cu_2WS_4 was totally quenched in the hydrogenated nanosheets, indicating the band gap of semiconducting pristine Cu_2WS_4 was closed upon hydrogenation.[26] It is interesting that the quenching of photoluminescence in hydrogenated-Cu_2WS_4 nanosheet can be kept even after temperature treatment at 350 °C (Figure S5), indicating robust metallicity in the hydrogenated-Cu_2WS_4 nanosheet. The above experimental results provide direct evidence for a semiconductor-to-metal transition between pristine Cu_2WS_4 and hydrogenated-Cu_2WS_4 nanosheets.

With its high conductivity metallic hydrogenated-Cu_2WS_4 nanosheet is a promising candidate for the construction of flexible nanodevices. We studied the electrochemical properties of hydrogenated-Cu_2WS_4 nanosheet by assembling it into a flexible supercapacitor in all-solid-state. The hydrogenated-Cu_2WS_4 nanosheet film assembled by a vacuum filtration method was transferred onto a gold-coated PET substrate as the working electrode for the symmetrical supercapacitor, and the thickness of the film electrode was estimated to be ca. 2 μm (Figure S6). Polyvinyl alcohol (PVA)–LiCl gel was used as solid-state polymer electrolyte. As expected, the as-fabricated all-solid-state supercapacitor exhibits excellent electrochemical performances (Figure 4). The CV curves are nearly rectangular including a wide hump in the voltage

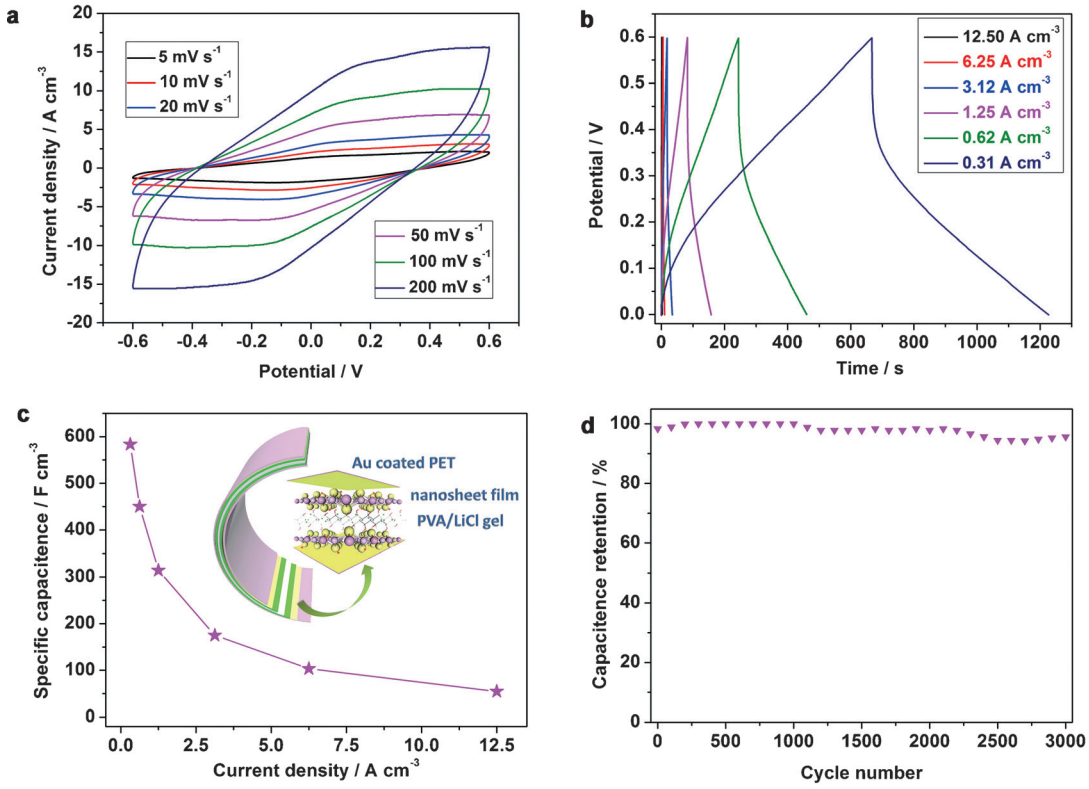

Figure 4. a) CV curves of the as-fabricated supercapacitor in PVA/LiCl electrolyte from −0.6 V to 0.6 V at different scan rates. b) Galvanostatic charge–discharge curves at different current density. c) Specific capacitance versus current density from 0.31 A cm^{-3} to 12.5 A cm^{-3}. The inset shows a schematic illustration of the structure of the as-fabricated symmetrical supercapacitor. d) Cycling behavior at 1.25 A cm^{-3}.

range from 0 to 0.6 V, and −0.6 to 0 V as well, indicating the co-existence of double-layered capacitive behavior and pseudocapacitive behavior of the electrode. In order to reveal the possible pseudocapacitive reactions of the hydrogenated-Cu_2WS_4 nanosheets during the charge–discharge process, XPS analysis on the electrode after charging from 0 to 0.6 V was carried out. As displayed in Figure S7 showing the Cu 2p spectra, the Cu^I centers in the hydrogenated-Cu_2WS_4 nanosheet are oxidized to Cu^{II} during charging, undergoing a reaction of $Cu^I - e^- \rightarrow Cu^{II}$. In this case, the capacitances of the as-designed supercapacitor were contributed by the synergistic effect between the double-layered capacitances and pseudocapacitive behavior of the hydrogenated-Cu_2WS_4 electrode. The galvanostatic charge–discharge measurements performed at current density from 0.31 $A\,cm^{-3}$ to 12.5 $A\,cm^{-3}$ are shown in Figure 4b, from which the specific capacitances were calculated (Figure 4c). The value of the specific capacitance is estimated to be 583.3 $F\,cm^{-3}$ at a current density of 0.31 $A\,cm^{-3}$, which can even retain up to 314.1 $F\,cm^{-3}$ at a high current density of 1.25 $A\,cm^{-3}$. We calculated an energy density of 0.029 $Wh\,cm^{-3}$ at a current density of 0.31 $A\,cm^{-3}$, giving a power density of 0.187 $W\,cm^{-3}$. At 1.25 $A\,cm^{-3}$, the energy and power densities of the electrode reach 0.016 $Wh\,cm^{-3}$ and 0.75 $W\,cm^{-3}$, respectively. These values are higher than that of previously reported all-solid-state supercapacitors (Figure S9). The as-fabricated supercapacitor is very stable in tests, retaining up to 95% of the initial capacitance after 3000 charge–discharge cycles. In addition, the supercapacitor exhibits excellent flexibility (Figure S8), showing negligible degradation in capacitance after 500 bending–extending cycles. In short, the hydrogenated-Cu_2WS_4 nanosheet with high conductivity would be an excellent electrode for the design of portable energy storage devices.

In conclusion, we demonstrate that the conductive nature of Cu_2WS_4 can be switched from semiconducting to metallic by hydrogen incorporation, accompanied by a highly improved electrical conductivity. The as-obtained ultrathin hydrogenated-Cu_2WS_4 nanosheet film exhibits superior electrical conductivity with a value of about $2.9 \times 10^4\ S\,m^{-1}$ at room temperature, which is almost 10^{10} higher than that of corresponding bulk sample. The as-fabricated flexible all-solid-state supercapacitor based on hydrogenated-Cu_2WS_4 nanosheet film exhibits extremely high electrochemical performances, indicating the metallic hydrogenated-Cu_2WS_4 nanosheet would be a promising electrode for the design of next-generation nanodevices. Our findings offer a practical way for the design of highly conductive electrodes, and provide a deep understanding of the electronic control in two-dimensional crystals through elemental doping.

Experimental Section

Fabrication of all-solid-state thin-film supercapacitor: The hydrogenated-Cu_2WS_4 film with 1 cm × 0.8 cm planar size and ca. 2 μm in thickness (0.24 $mg\,cm^{-2}$ in mass loading density) was transferred onto a gold-coated PET sheet (1.5 cm × 3 cm), both operating as the two electrodes in a symmetrical supercapacitor. Gold-coated polyethylene terephthalate (PET) sheets were used as the flexible substrate and current collector. PVA/LiCl gel was introduced as the solid electrolyte and separator. After careful sealing, the flexible all-solid-state thin-film supercapacitor was successfully assembled.

Acknowledgements

This work was supported by the National Basic Research Program of China (2015CB932302), the National Natural Science Foundation of China (U153226, 21401181, 21331005, 11321503, 91422303), the Fundamental Research Funds for the Central University (WK2060190027, WK2340000063), the Key Laboratory of Neutron Physics (CAEP, 2014DB01), and a Scientific Research Grant of the Hefei Science Center of CAS (2015HSC-UE006, 2015HSC-UP015).

Keywords: electrical conductivity · all-solid-state supercapacitor · hydrogen incorporation · ternary chalcogenides · nanosheets

How to cite: *Angew. Chem. Int. Ed.* **2016**, *55*, 5733–5738
Angew. Chem. **2016**, *128*, 5827–5832

[1] X. Zhang, Y. Xie, *Chem. Soc. Rev.* **2013**, *42*, 8187.
[2] X. Huang, Z. Zeng, H. Zhang, *Chem. Soc. Rev.* **2013**, *42*, 1934.
[3] C. Wu, X. Lu, L. Peng, K. Xu, X. Peng, J. Huang, G. Yu, Y. Xie, *Nat. Commun.* **2013**, *4*, 2431.
[4] M. Ghidiu, M. R. Lukatskaya, M.-Q. Zhao, Y. Gogotsi, M. W. Barsoum, *Nature* **2014**, *516*, 78.
[5] X. Zhang, X. Xie, H. Wang, J. Zhang, B. Pan, Y. Xie, *J. Am. Chem. Soc.* **2013**, *135*, 18.
[6] Y. Sun, H. Cheng, S. Gao, Z. Sun, Q. Liu, Q. Liu, F. Lei, T. Yao, J. He, S. Wei, Y. Xie, *Angew. Chem. Int. Ed.* **2012**, *51*, 8727; *Angew. Chem.* **2012**, *124*, 8857.
[7] C. N. R. Rao, H. S. S. Ramakrishna Matte, U. Maitra, *Angew. Chem. Int. Ed.* **2013**, *52*, 13162; *Angew. Chem.* **2013**, *125*, 13400.
[8] E. Scalise, M. Houssa, G. Pourtois, V. Afanasev, A. Stesmans, *Nano Res.* **2012**, *5*, 43.
[9] M. A. Lukowski, A. S. Daniel, F. Meng, A. Forticaux, L. Li, S. Jin, *J. Am. Chem. Soc.* **2013**, *135*, 10274.
[10] W.-H. Xie, Y.-Q. Xu, B.-G. Liu, D. G. Pettifor, *Phys. Rev. Lett.* **2003**, *91*, 037204.
[11] C. Lin, X. Zhu, J. Feng, C. Wu, S. Hu, J. Peng, Y. Guo, L. Peng, J. Zhao, J. Huang, J. Yang, Y. Xie, *J. Am. Chem. Soc.* **2013**, *135*, 5144.
[12] G. Eda, G. Fanchini, M. Chhowalla, *Nat. Nanotechnol.* **2008**, *3*, 270.
[13] X. Li, G. Zhang, X. Bai, X. Sun, X. Wang, E. Wang, H. Dai, *Nat. Nanotechnol.* **2008**, *3*, 538.
[14] W. Chen, Y. Li, G. Yu, C.-Z. Li, S. B. Zhang, Z. Zhou, Z. Chen, *J. Am. Chem. Soc.* **2010**, *132*, 1699.
[15] D. Voiry, H. Yamaguchi, J. Li, R. Silva, D. C. B. Alves, T. Fujita, M. Chen, T. Asefa, V. B. Shenoy, G. Eda, M. Chhowalla, *Nat. Mater.* **2013**, *12*, 850.
[16] H. Wang, J. Zhang, X. Hang, X. Zhang, J. Xie, B. Pan, Y. Xie, *Angew. Chem. Int. Ed.* **2015**, *54*, 1195; *Angew. Chem.* **2015**, *127*, 1211.
[17] D. C. Elias, R. R. Nair, T. M. G. Mohiuddin, S. V. Morozov, P. Blake, M. P. Halsall, A. C. Ferrari, D. W. Boukhvalov, M. I. Katsnelson, A. K. Geim, K. S. Novoselov, *Science* **2009**, *323*, 610.
[18] K. Ramasamy, H. Sims, W. H. Butler, A. Gupta, *J. Am. Chem. Soc.* **2014**, *136*, 1587.
[19] H. Li, X. Duan, X. Wu, X. Zhuang, H. Zhou, Q. Zhang, X. Zhu, W. Hu, P. Ren, P. Guo, L. Ma, X. Fan, X. Wang, J. Xu, A. Pan, X. Duan, *J. Am. Chem. Soc.* **2014**, *136*, 3756.

[20] P. D. Tran, M. Nguyen, S. S. Pramana, A. Bhattacharjee, S. Y. Chiam, J. Fize, M. J. Field, V. Artero, L. H. Wong, J. Loo, J. Barber, *Energy Environ. Sci.* **2012**, *5*, 8912.
[21] C. J. Crossland, P. J. Hickey, J. S. O. Evans, *J. Mater. Chem.* **2005**, *15*, 3452.
[22] D. Jing, M. Liu, Q. Chen, L. Guo, *Int. J. Hydrogen Energy* **2010**, *35*, 8521.
[23] C. J. Crossland, J. S. O. Evans, *Chem. Commun.* **2003**, 2292.
[24] H. Chen, K. Zhang, W. Chen, I. Ali, P. Wu, D. Liu, L. Song, *AIP Adv.* **2015**, *5*, 037141.
[25] M. Sardo, R. Siegel, S. M. Santos, J. Rocha, J. R. B. Gomes, L. Mafra, *J. Phys. Chem. A* **2012**, *116*, 6711.
[26] S. S. Chou, Y.-K. Huang, J. Kim, B. Kaehr, B. M. Foley, P. Lu, C. Dykstra, P. E. Hopkins, C. J. Brinker, J. Huang, V. P. Dravid, *J. Am. Chem. Soc.* **2015**, *137*, 1742.

Received: January 3, 2016
Published online: April 6, 2016

